Metrol. Meas. Syst., Vol. 32 (2025) No. 4, pp. 1–23
DOI: 10.24425/mms.2025.155807

PAN POLSKA AKADEMIA NAUK

METROLOGY AND MEASUREMENT SYSTEMS
Index 330930, ISSN 0860-8229
www.metrology.wat.edu.pl

M&MS

A BASELINE-FREE MULTIMODAL PIPE DAMAGE IDENTIFICATION METHOD BY MACHINE LEARNING

Mingyuan Wang, Yiqing Gu, Yaokai Li, Jiuhong Jia, Shan-Tung Tu

Key Laboratory of Pressure Systems and Safety, Ministry of Education,
East China University of Science and Technology, Shanghai, China (✉ *jhjia@ecust.edu.cn*)

Abstract

Structural Health Monitoring (SHM) of pipe infrastructures is of paramount importance to prevent catastrophic failures induced by defects such as corrosion. Conventional damage identification methodologies are frequently faced with challenges, including baseline dependency, limitations inherent in single-sensor data, and considerable economic expenditure. This paper presents a novel, baseline-free, multi-modal damage identification methodology developed for Level 3 assessment of multiple damages, encompassing their detection, localisation, and quantification. Initially, Level 1 damage identification is accomplished through observation of the Regional Resonance Pair (RRP) phenomenon. Subsequently, potential damage regions are predicted by a Multilayer Perceptron (MLP) model that uses vibration modal frequencies, generating a Macro-F1 score of 0.8131 on the test set; this prediction is then integrated with a high-precision local point cloud, acquired via Line Structured Light (LSL) technology, to achieve precise Level 2 damage location, with a reported error as low as 1.78%. Following localisation, Level 3 quantification of the damage is performed using point cloud registration, fusion, and voxelisation techniques, enabling accurate prediction of damage volume with a quantification error of merely 2.47%.

Keywords: regional resonance pair, multiple damage, line structured light, multimodal, vibration modal analysis.

1. Introduction

Structural Health Monitoring (SHM) of infrastructure, such as pipes, constitutes an extensive and significant field of research, primarily focused on the identification of structural defects, monitoring of structural conditions, and assessment of structural safety based on sensor data [1–3]. Pipes are frequently situated in corrosive environments and, with continued usage, undergo an aging process that could precipitate pipe failure [4, 5], thereby engendering severe environmental and socio-economic ramifications [6]. Corrosive defects not only inflict substantial environmental damage but also incur considerable maintenance costs [7]. This inevitable process underscores the importance of early damage identification and maintenance, as structural damage typically induces alterations in its dynamic characteristics, consequently affecting modal properties.

Article history: received June 9, 2025; revised September 16, 2025; accepted October 22, 2025; available online December 09, 2025.

To mitigate economic losses, researchers have proposed various global and local damage identification methods [8–10]. Global methods are generally based on the vibrational characteristics of the pipe [11–14], whereas local methods use a point cloud acquired by cameras as an alternative to traditional visual inspection techniques [15–17]. This paper proposes a scheme for the further assessment of the severity of local damage using data derived from global methods, in contrast to conventional damage identification methods that rely on baseline [18, 19].

The damage identification process typically encompasses three principal stages: detection, localisation, and quantification. Within these stages, classification methods based in *Machine Learning* (ML) have been favoured by researchers [20–23] to further improve the accuracy of damage identification. Methodologies such as *Artificial Neural Networks* (ANN) [24], *Support Vector Machines* (SVM) [25], *Logistic Regression* (LR) [26], *Random Forests* (RF) [27], and *eXtreme Gradient Boosting* (XGB) [28] have been extensively applied in these tasks. With the continuously increasing demand for SHM, the development of more efficient and robust identification methods is urgently required to construct ML models capable of correlating extracted damage-sensitive features with damage detection.

Multi-modal identification methods, through the integration of data from disparate sources, could effectively address certain limitations encountered by traditional single-sensor approaches. For instance, reliance solely on vibration modal analysis can result in incomplete or erroneous measurement data due to environmental factors or improper sensor deployment [29–31]. In contrast, if all damage assessments depend entirely on 3D scanning, the cost of identification would be significantly elevated [32–34]. Compared to conventional methods, the adoption of multi-modal methods could markedly improve the precision and reliability of damage identification [35], as it synthesises information provided by different signal sources, thus enhancing the capability to recognise damage.

To address this issue, the present study proposes a multi-modal damage identification method that combines vibration modal analysis with Line Structured Light (LSL) technology. By amalgamating dynamic response data from vibration modal analysis with a 3D surface point cloud from LSL, this approach not only compensates for the deficiencies of individual techniques, but also enables complementarity between different data sources, further augmenting the accuracy and reliability of identification. In this paper, ML classification algorithms are also effectively applied in Level 2 damage localisation, which, when combined with LSL, facilitates rapid and precise localisation of specific damage sites. ML algorithms can establish the relationship between damage localisation bands and modal frequencies, and they enhance the efficiency and intelligence level of damage identification.

In prior research [11], during vibration modal testing of pipes with single damage, the *Regional Resonance Pair* (RRP) phenomenon is observed, as illustrated in Fig. 1. Damage disrupts the axial symmetry of the pipe, leading to a divergence in the originally identical modal frequencies of an RRP, thereby forming active and passive components, denoted by subscripts A and P, respectively. The primary focus of the current study is the influence of multiple non-axisymmetric damages on the vibrational modes of pipes, and a Level 3 multiple-damage identification method applicable to clamped-clamped pipes is proposed. The method integrates vibration analysis, machine learning, and 3D laser scanning as shown in Fig. 2. The process starts with a modal test to acquire vibration data. First, if a specific frequency ratio is less than 1.0, damage is confirmed; otherwise, a detection method based on LSL is activated. Next, if the centroid cannot be found within a predefined tolerance, a machine learning model is deployed to predict a general damage location band. Finally, the damage is quantified by creating a unified 3D point cloud from multiple LSL scans and applying voxelisation [36] to calculate its precise volume. Compared to traditional methods, this approach significantly enhances the efficiency of detecting multiple damages. Specifically, the

damage localisation bands of the pipe are first predicted using an ML model; subsequently, depth information is extracted from the point cloud, and data from different sources are fused, ultimately enabling the prediction of damage volume. The efficacy of this method is validated through modal hammer excitation tests and LSL scanning experiments, revealing high accuracy across all three stages of damage detection, localisation, and quantification.

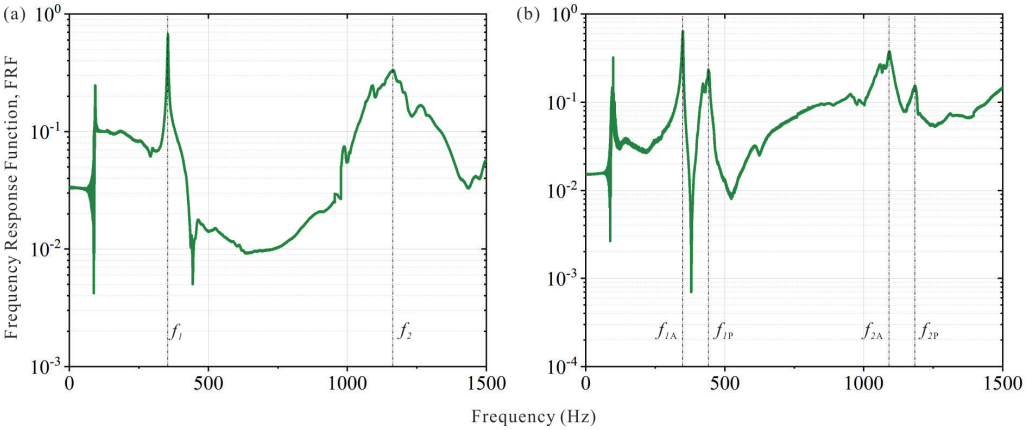

Fig. 1. Regional resonance pair examples of the pipe: (a) undamaged, (b) non-axisymmetrically damaged.

2. Methodology

2.1. Overview

To effectively address the problem of multiple damage identification in pipes, this study proposes a novel Level 3 identification method based on pipe modal frequencies and LSL; the specific workflow of this method is illustrated in Fig. 2. The determination of damage presence, designated as Level 1 damage identification, is based on the observation of the RRP phenomenon within the acquired pipe modal frequencies. If such a phenomenon is present, LSL is employed exclusively within the region up to 0.1L0 of the pipe to localise the damage centroid position. This focused application is necessary because the constructed damage localisation bands are incapable of detecting damage within this 0.1L0 proximal region. L0 represents the effective length of the pipe. Level 2 damage identification involves addressing the multi-label classification problem for damage localisation bands through ML, thereby establishing a relationship between damage localisation band labels and the pipe's modal frequencies and their ratios. Subsequently, the rapid acquisition of the damage centroid position is achieved by utilising LSL to gather pipe depth information. For Level 3 damage identification, point clouds acquired by monocular LSL are registered and fused. The damage centroid position obtained from Level 2 is then conveyed to the point cloud voxelisation process, which ultimately enables the prediction of the volume of the damaged pipe section.

The training procedure and algorithm selection for the ML model are illustrated in Fig. 3. This process comprises three principal stages: model training, threshold optimisation, and model inference. Initially, feature extraction is performed, in which various features (*e.g.*, frequency ratios) are extracted from the input data. The annotation of the damage localisation band is subsequently conducted based on predefined damage states (*e.g.*, [0, 1, 0, 0, 0, 1]). The training set

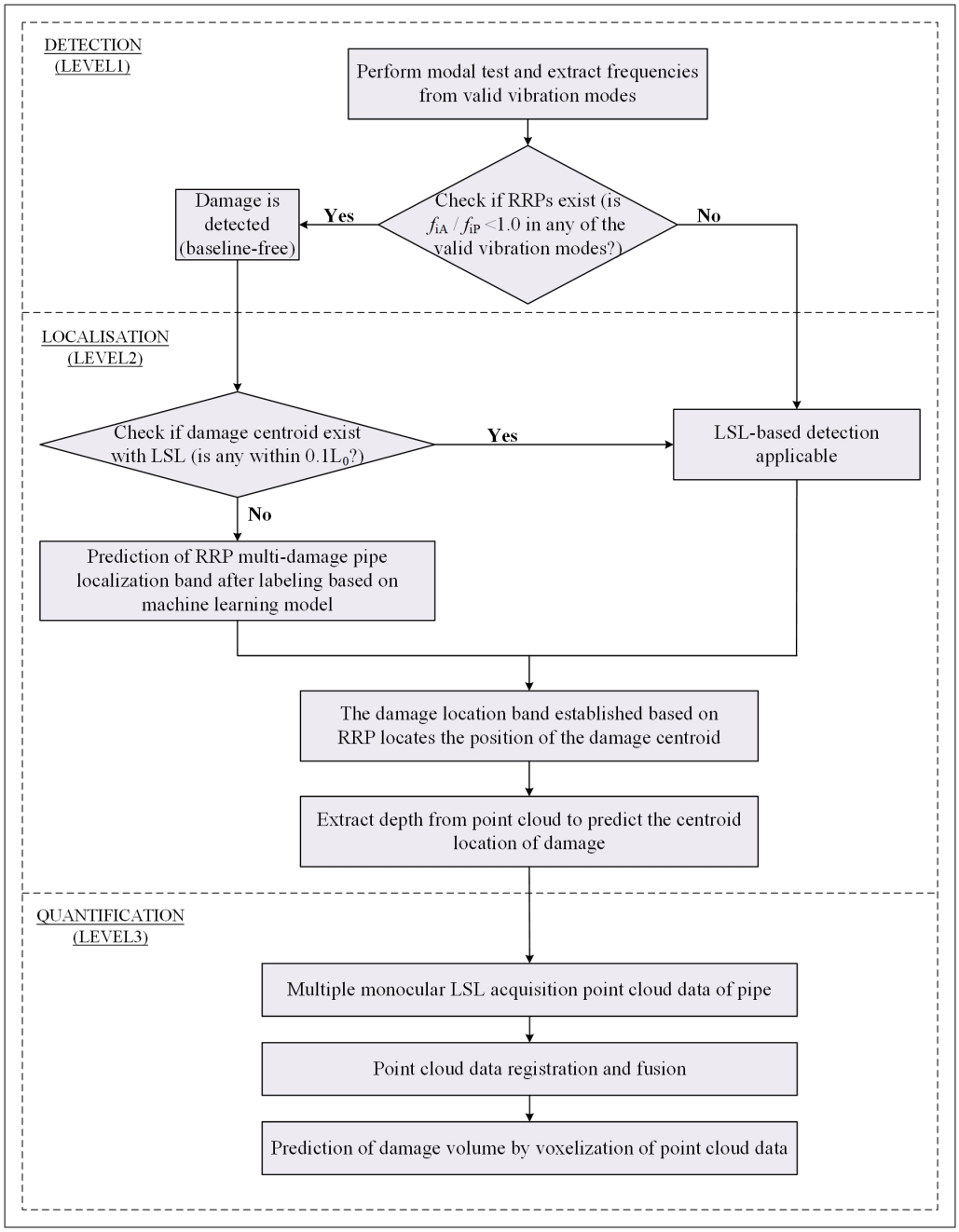

Fig. 2. Flowchart of the multiple damage identification method (detection, localisation, and quantification) in pipes.

is then subjected to standardisation to ensure data homogeneity. Finally, a One-vs-Rest algorithm is configured and trained; this model is designated for handling multi-class classification problems. The trained model is used to predict the probabilities in the validation set, and based on these

predictions, an optimal threshold is searched. To enhance the model's generalisability in practical applications, the list of optimal thresholds for each damage localisation band is preserved for subsequent utilisation during the inference phase. The test set is standardised to ensure its similarity with the training set data. The probabilities are then predicted for the test set using the trained model. Subsequently, by applying the previously preserved thresholds to these predicted probabilities, the damage localisation band label for each data point is determined and the set of damage localisation band labels is eventually outputted.

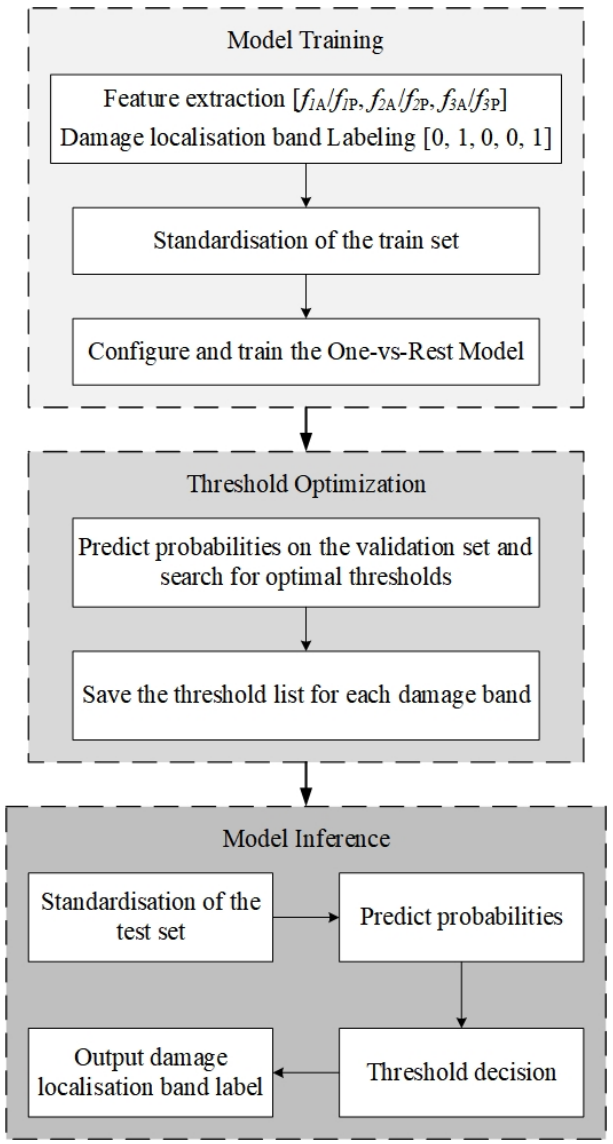

Fig. 3. Machine learning workflow for predicting damage localisation bands and optimisation of thresholds.

2.2. RRP

The *Regional Resonance Pair* (RRP) describes a specific physical vibration phenomenon that arises from local damage in a structure. In an ideal, undamaged, and symmetrical structure, such as a uniform pipe, a particular vibration mode typically corresponds to a single, well-defined resonant frequency. However, when a local defect (such as a corrosion pit, crack, or dent) is introduced, it breaks the physical symmetry at that location. This disruption of symmetry causes the original single vibration mode to split into two new vibration modes that are very close in energy but have slightly different frequencies. This pair of new resonant frequencies, which are induced by the damage and appear together with extremely close frequency values, is defined as a "resonance pair".

The term "regional" highlights another critical physical property of this phenomenon: its localised nature. Unlike an undamaged structure, where vibrational energy is distributed throughout the entire body, the energy associated with this new resonance pair becomes highly concentrated in the confined area around the damage point that caused the frequency split. In other words, when the structure vibrates at these two specific frequencies, the point of maximum amplitude and energy concentration coincides exactly with the location of the physical damage. Consequently, an RRP is more than just a pair of frequency values; it represents a localised vibrational state that is strongly correlated with the damage location, inherently carrying physical information about the position of the defect itself. For the RRP discovery process, please refer to the previous research [11].

The pipe damage localisation bands are predicated upon the ranking of RRPs for pipes exhibiting a single damage, in conjunction with the ranking of intercepts obtained from the linear fitting of damage volume. The five resulting damage localisation bands are depicted in Fig. 4. The RRP ranking for pipes with single damage centroids at various locations is simulated; a change in the RRP ranking signifies a corresponding alteration in the damage localisation band. The boundary between two adjacent damage localisation bands is consequently defined as the average of the two damage centroid positions associated with this change. As illustrated in Fig. 4, the centroid positions selected for the simulation spanned from 0.1L0 to 0.5L0, with an incremental step size of 0.05L0. Given that pipes with fixed-fixed boundary conditions are chosen as the subject of this investigation, the overall pipe structure is inherently axisymmetric. Consequently, the damage localisation bands also exhibit axial symmetry, as shown in Fig. 4.

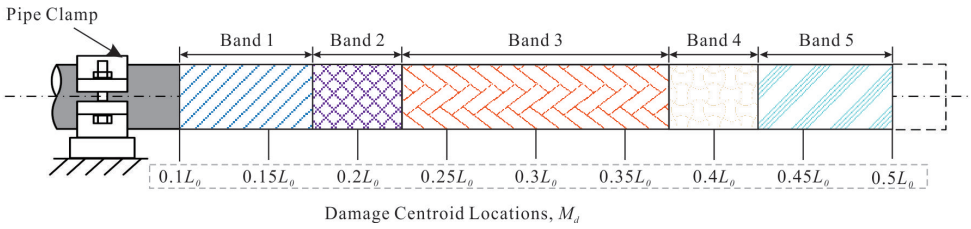

Fig. 4. Five damage localisation bands for a clamped-clamped pipe.

2.3. Multiple-damage pipe

In practical service, pipes commonly encounter issues related to multiple damages; therefore, this study employs scenarios involving multiple damages to assess the applicability of the method illustrated in Fig. 1. The parameters for a pipe with two damages are defined as shown in Fig. 5. The positions of the two damage centroids are denoted by M_{d1} and M_{d2}, respectively; the damage depths are T_{d1} and T_{d2}; the damage lengths are L_{d1} and L_{d2}; the angles corresponding to the damages are α_{d1} and α_{d2}; and the angle between the two damage centroids is β.

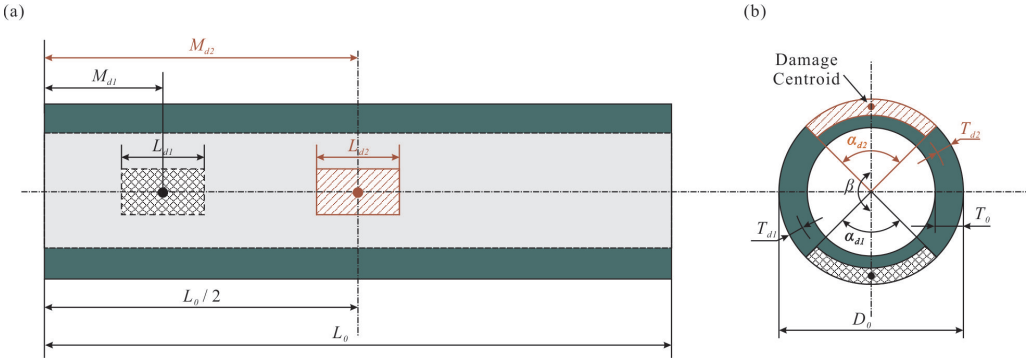

Fig. 5. Damage parameters for a pipe with double damage: (a) axial, (b) radial.

The parameters for a pipe with three damages are defined as depicted in Fig. 6. The positions of three damage centroids are represented by M_{d1}, M_{d2}, and M_{d3}, respectively; the damage depths are T_{d1}, T_{d2}, and T_{d3}; and the damage lengths are L_{d1}, L_{d2}, and L_{d3}; the angles corresponding to the instances of damages are α_{d1}, α_{d2}, and α_{d3}. Due to the increased complexity of combinations involving three damages compared to two, and the prerequisite of first validating the RRP phenomenon for multiple-damage pipes, the subsequent database construction in this paper will be confined to pipes with two damages. For pipes with three damages, a specific scenario is constructed wherein the angle between each of the three damage centroids is 60°. This configuration is intended to validate the phenomenon of modal aliasing in high-frequency modes, which is posited to occur when three damage centroids are equidistantly spaced, according to theoretical research on circumferential modes [37, 38].

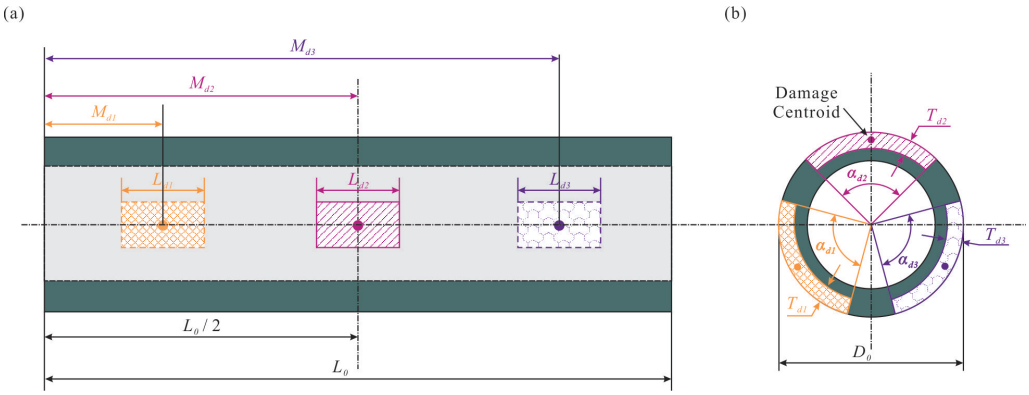

Fig. 6. Damage parameters for a pipe with triple damage: (a) axial, (b) radial.

The damage parameter settings for the database are detailed in Table 1. To conserve computational resources while simultaneously verifying the applicability of the proposed method, this study used the principles of Uniform Design experimentation. Specifically, Latin hypercube sampling is utilised to generate 1000 distinct sets of conditions, intended to represent the entirety of possible combinations. In this design, the two damages are configured to ensure mutual non-interference, *i.e.*, the distance between their respective centroids is consistently maintained at a value greater than half the sum of their lengths. It is generally acknowledged that the occurrence of two identically

configured damages is highly improbable in real-world scenarios; consequently, the dimensions of the two damages are not set to be exactly the same. Existing theoretical research on circumferential modes [39] has indicated a propensity to modal aliasing when the angle β between two damages is either 90° or 180°; therefore, these two specific angular configurations are excluded. These operations are implemented through automated Python scripting for Ansys Discovery and Ansys Mechanical.

Table 1. Parameters of damaged pipes in the database.

M_{d1} (mm)	α_{d1} (°)	T_{d1} (mm)	L_{d1} (mm)	β (°)	M_{d2} (mm)	α_{d2} (°)	T_{d2} (mm)	L_{d2} (mm)
90	22.5	1.30	40	30	517.5	22.5	1.30	40
180	45	2.60	80	60	540	45	2.60	80
270	67.5	3.90	120	120	630	67.5	3.90	120
360	90	5.20	–	150	720	90	5.20	–
382.5	–	–	–	–	810	–	–	–

3. Experiment with a multiple-damage pipe

3.1. Test setup

A total of two experiments are configured in this study: one is the modal hammer excitation test mentioned above, and the other is a monocular LSL scanning experiment. These two experiments collectively constitute the Level 3 damage identification method proposed herein. For both experiments, pipes made of AL 6063 T5 material are selected. The undamaged pipe, designated as Pipe 1, possessed an effective length L_0 of 900 mm, an outer diameter of 103 mm, and a wall thickness of 6.5 mm. The volume of this undamaged pipe is determined to be 1734630.384 mm^3, a value that will be used for subsequent Level 3 damage quantification error calculations. Furthermore, the active component of the i-th RRP of the pipe is denoted by f_{iA}, and the passive component by f_{iP}. For subsequent modal and mode shape analysis of multiple-damage pipes, the first three pairs of RRPs for this undamaged pipe are obtained through simulation as 542.63 Hz, 1318.6 Hz, and 2283.1 Hz, *i.e.*, $f_{1A} = f_{1P} = 542.63$ Hz, $f_{2A} = f_{2P} = 1318.6$ Hz, and $f_{3A} = f_{3P} = 2283.1$ Hz. The parameter settings for the double-damage and triple-damage pipes employed in the modal hammer excitation tests are presented in Table 2 and Table 3, respectively.

Table 2. Parameters of a double-damage pipe under modal excitation test, where *dbl* is double damage.

Pipe Label	Test Case	M_{d1} (mm)	α_{d1} (°)	T_{d1} (mm)	L_{d1} (mm)	M_{d2} (mm)	α_{d2} (°)	T_{d2} (mm)	L_{d2} (mm)	β (°)	δ (°)
2	2a_dbl	200	30	2	100	450	60	4	50	30	0
	2b_dbl										45
	2c_dbl										90
3	3a_dbl									60	0
	3b_dbl										45
	3c_dbl										90
4	4a_dbl									120	0
	4b_dbl										45
	4c_dbl										90
5	5a_dbl									150	0
	5b_dbl										45
	5c_dbl										90

Table 3. Parameters of triple-damage pipe in modal excitation test, where *trp* is triple damage.

Pipe Label	**6**		
Test Case	6a_trp	6b_trp	6c_trp
M_{d1} (mm)	200		
α_{d1} (°)	30		
T_{d1} (mm)	2		
L_{d1} (mm)	100		
M_{d2} (mm)	450		
α_{d2} (°)	60		
T_{d2} (mm)	4		
L_{d2} (mm)	50		
M_{d3} (mm)	700		
α_{d3} (°)	90		
T_{d3} (mm)	3		
L_{d3} (mm)	80		
δ (°)	0	45	90

Previous research [11] had already observed the RRP phenomenon in pipes with a single damage. The RRP phenomenon in multiple-damage pipes is further investigated through modal hammer excitation; the setup for this modal hammer excitation experiment is illustrated in Fig. 7. Figure 7(a) shows the angle δ formed by the accelerometer and the damage, as well as the direction of the excitation of the modal hammer. Figure 7(b) shows all the equipment used in the entire experimental platform. The positions of the six accelerometers are established at 150 mm, 250 mm, 350 mm, 450 mm, 650 mm, and 750 mm. This sensor placement strategy is designed to avoid the node point of the vibration modes identified in the simulation results, thereby facilitating a more effective observation of the mode shape test results. Moreover, to prevent significant deviations in the frequency response, the occurrence of double hits, as illustrated in Fig. 8, must be avoided when exciting the pipe with the modal hammer; specifically, the double-hit scenario depicted in Fig. 8(a) should be averted.

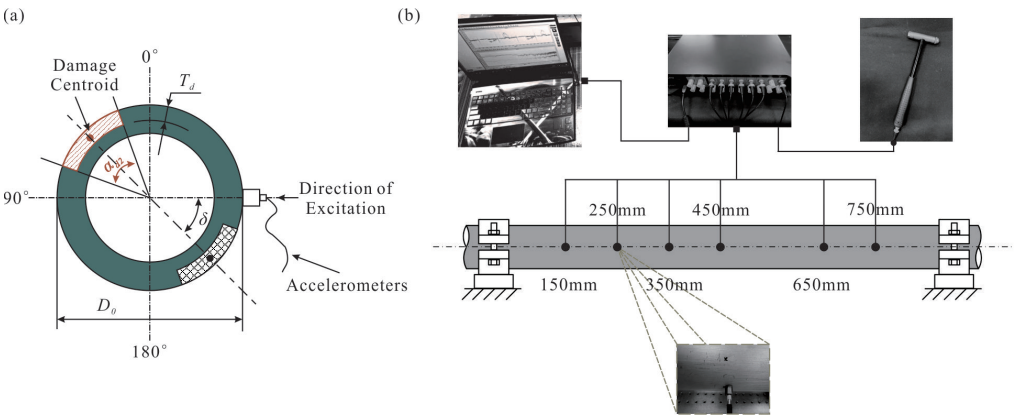

Fig. 7. Modal hammer excitation test setup: (a) location of accelerometers, (b) layout of other equipment.

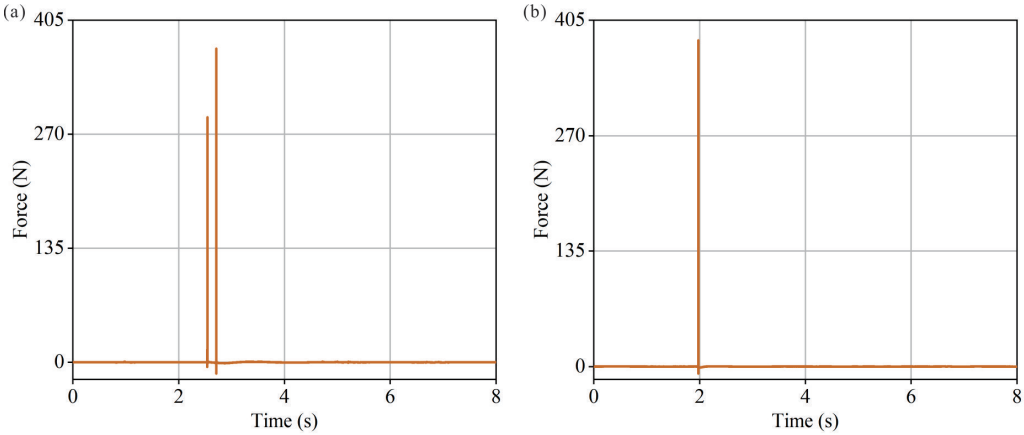

Fig. 8. Time domain signal of modal hammer excitation: (a) double, (b) normal.

In the monocular LSL experiment, two industrial cameras are employed to scan a partial point cloud of the same pipe from two distinct angles. This experiment is designed to validate whether LSL could quantify multiple damages; consequently, only the damage at the M_{d1} position is scanned. The process for multiple damages would merely involve repeating the scanning procedure based on the localisation results. The damage centroid is positioned at 200 mm; the damage length is 125 mm; its central angle is 90°, and its depth is 4 mm. All equipment used is shown in Fig. 9. During the scanning process, the laser and the industrial cameras were kept in a stationary position, while a servo motor drove a sliding stage to move the pipe horizontally at a set speed of 1 mm/s. The industrial cameras acquired an image every 0.1 seconds, resulting in a point cloud precision of 0.1 mm. All point clouds obtained from monocular LSL scanning are processed using Python for registration, fusion, and voxelisation.

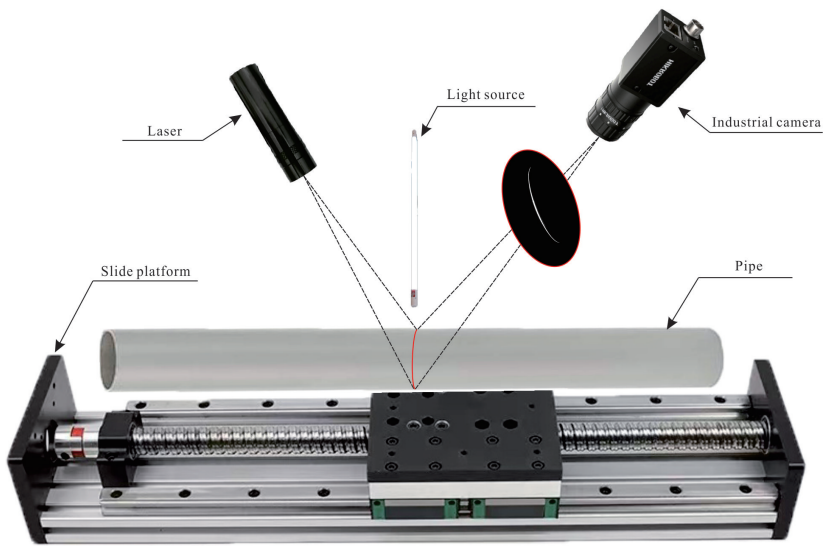

Fig. 9. Test setup for monocular line structured light.

Point cloud preprocessing encompassed downsampling, normal vector estimation, and outlier removal. Voxel downsampling is utilised to reduce the point cloud density from over two million points to approximately 3000 points. The normal vector for each point is calculated for subsequent analysis, and noise points are removed through statistical filtering. Subsequently, the *Iterative Closest Point* (ICP) method, provided by CloudCompare, is employed to complete the registration operation. Finally, overlapping regions are detected, and a weighted average is applied to these overlapping regions, followed by a removal of duplicate points to maintain point cloud quality. Furthermore, during the prediction of damage volume via point cloud voxelisation, potential depression points are first identified by examining the radial distance from points to the pipe centroid, based on the results for Level 2 damage centroid localisation.

3.2. Modal analysis and damage detection

The test results of the modal hammer excitation experiments for the six pipes are presented in Fig. 10, where Fig. 10(a) displays the test results for the undamaged pipe, serving as a reference for observing the RRP phenomenon in multiple-damage pipes. During testing, the RRP phenomenon in multiple-damage pipes is more effectively observed by varying the angle between the accelerometer and the damage. Different observation effects for different vibration mode RRPs are noted at varying angles. As shown in Figs. 10(b) to 10(f), the RRP patterns of multiple-damage pipes could be more comprehensively analysed. The results of the modal test for the six pipes reveal that the deviation between the active and passive components of the first RRP is minimal, as detailed in Table 4. This indicates that multiple damages increase the resonance interval, *i.e.*, they enlarge the difference between the active and passive parts of the RRP.

Table 4. Frequency values of the RRP modal tests for the first four pairs of six pipes.

Test Case	**Mode 1 (Hz)**			**Mode 2 (Hz)**			**Mode 3 (Hz)**			**Mode 4 (Hz)**		
	f_{1A}	f_1	f_{1P}	f_{2A}	f_2	f_{2P}	f_{3A}	f_3	f_{3P}	f_{4A}	f_4	f_{4P}
1	–	355	–	–	1164	–	–	2180	–	–	3613	–
2a_dbl	363	–	457	–	–	–	–	–	–	–	–	–
2b_dbl	–	–	–	1009	–	1315	–	–	–	–	–	–
2c_dbl	–	–	–	–	–	–	2163	–	2518	3012	–	3603
3a_dbl	–	–	–	–	–	–	2117	–	2516	3074	–	3618
3b_dbl	–	–	–	1005	–	1294	–	–	–	–	–	–
3c_dbl	358	–	458	–	–	–	–	–	–	–	–	–
4a_dbl	–	–	–	–	–	–	2156	–	2522	3077	–	3661
4b_dbl	–	–	–	1020	–	1301	–	–	–	–	–	–
4c_dbl	358	–	459	–	–	–	–	–	–	–	–	–
5a_dbl	–	–	–	976	–	1285	–	–	–	–	–	–
5b_dbl	361	–	457	–	–	–	–	–	–	–	–	–
5c_dbl	–	–	–	–	–	–	2152	–	2514	2981	–	3597
6a_trp	–	–	–	–	–	–	2093	–	2530	3073	–	3637
6b_trp	362	–	459	–	–	–	–	–	–	–	–	–
6c_trp	–	–	–	960	–	1302	–	–	–	–	–	–

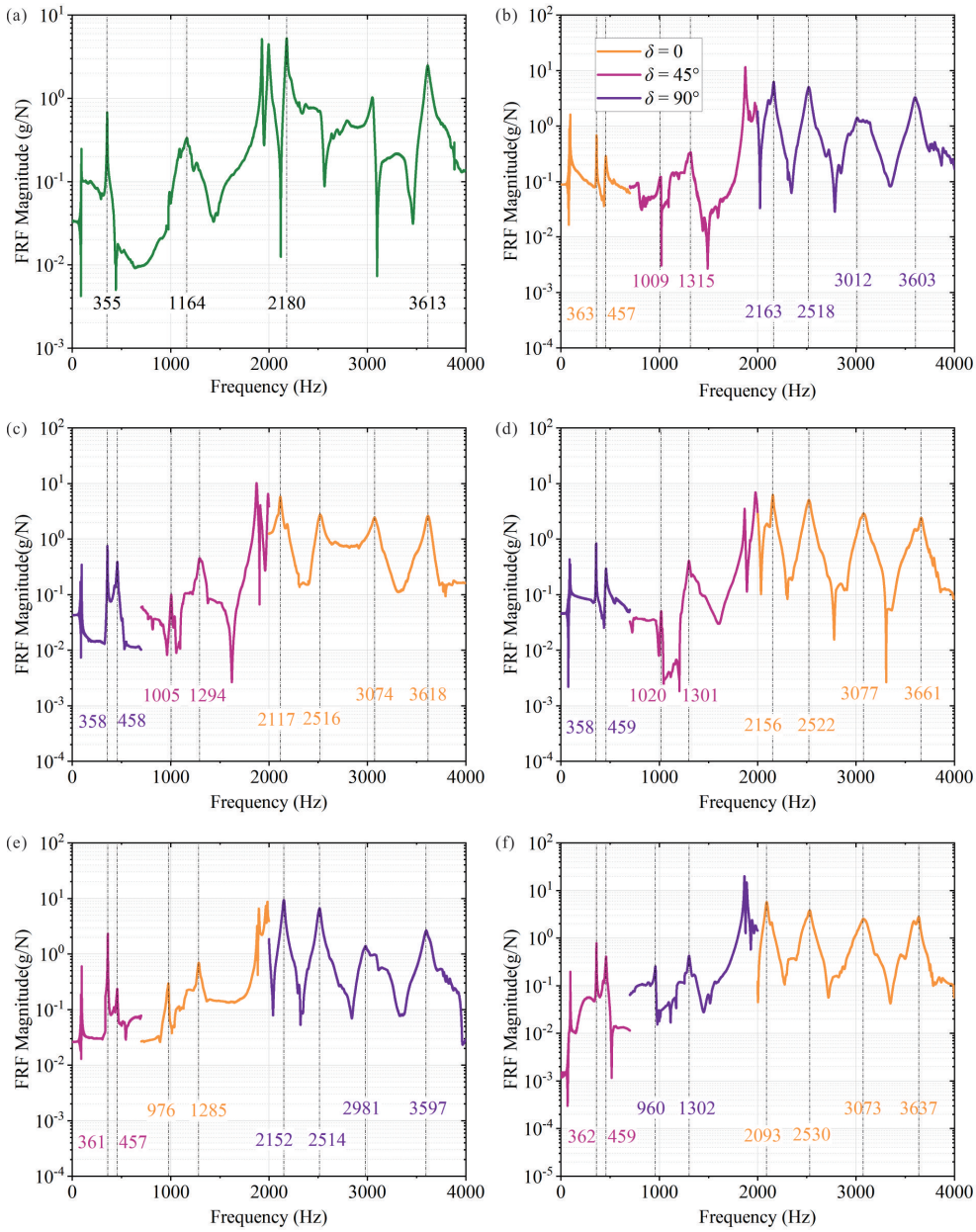

Fig. 10. Results of the RRP modal test of the first four pairs of six pipes: (a) undamaged, (b) Pipe 2, (c) Pipe 3, (d) Pipe 4, (e) Pipe 5, and (f) Pipe 6.

Although the mode shape results for the multiple-damage pipes exhibit considerable similarity to those of the undamaged pipe, as depicted in Fig. 11 (where $NP_{i,j}$ represents the j-th node of the i-th RRP), it is still necessary to incorporate the calculation results of the *modal assurance criterion* (MAC) [40] to ascertain whether modal aliasing has occurred, as shown in Fig. 12. The results indicate that the fourth RRP has already deviated from the modal shape of the undamaged

pipe. This suggests that low-frequency modes are consistent with previous theoretical research, while two damages can lead to modal aliasing in high-frequency modes [37]. For example, in Table 4, a significant difference could be observed between the frequency of the active part of the fourth RRP and that of the undamaged pipe, while the frequency difference of the passive part of the RRP relative to the undamaged pipe is considerably smaller. This is in contrast to the results for the other three RRPs, implying that the experimental results for the fourth RRP will not be included in the subsequent damage identification.

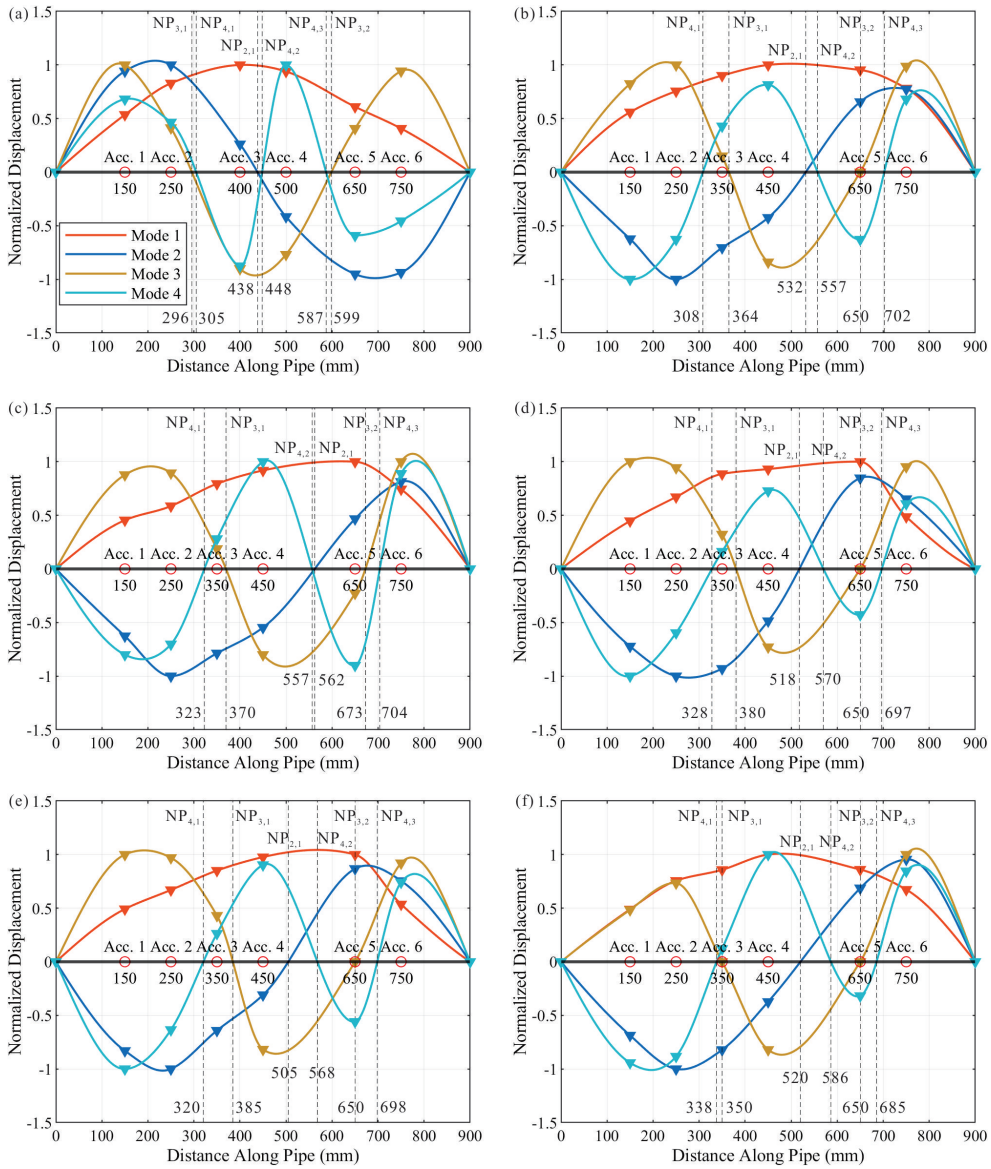

Fig. 11. Mode shape results for six pipes: (a) undamaged, (b) Pipe 2, (c) Pipe 3, (d) Pipe 4, (e) Pipe 5, and (f) Pipe 6.

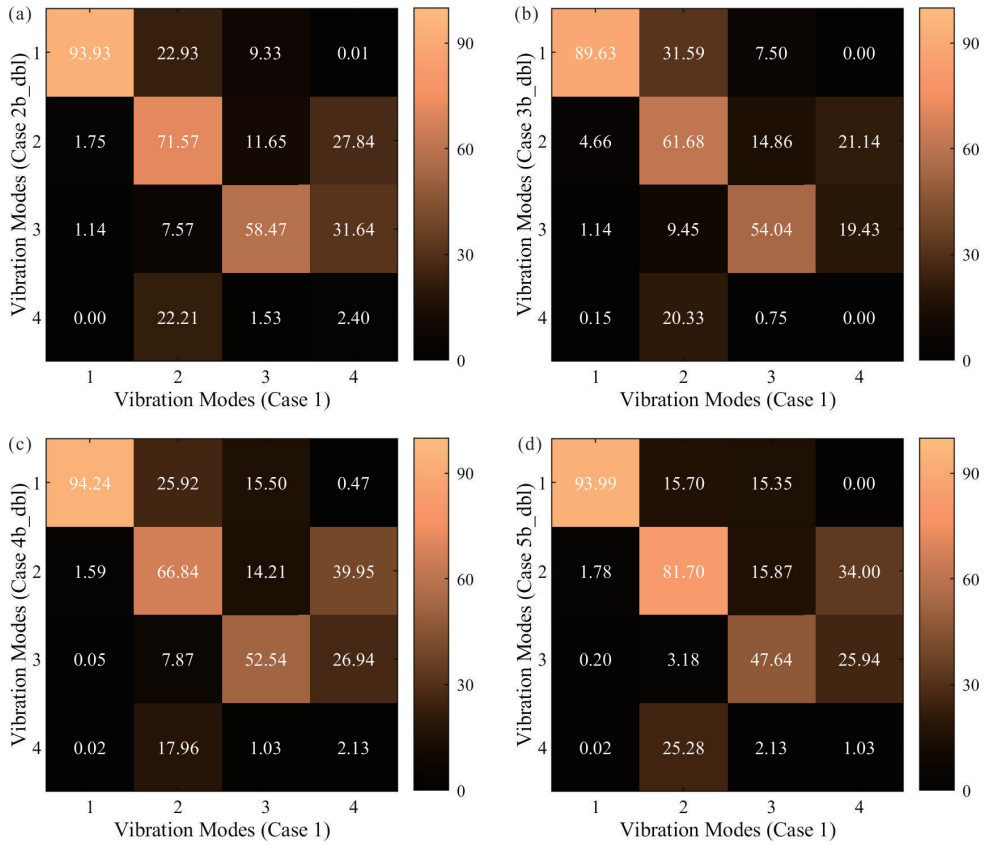

Fig. 12. MAC of vibration mode shapes for double-damage pipes and an undamaged pipe.

Furthermore, research findings [37] have indicated that three equidistantly spaced damage centroids exacerbate modal aliasing in high-frequency modes, as illustrated in Fig. 13. However, such equidistant spacing is rarely encountered in practical situations; therefore, this issue does not interfere with the applicability of the method proposed in this study. MAC calculations are also performed on the mode shape results of the active and passive parts of the four RRPs of a multiple-damage pipe, as shown in Fig. 14. The results demonstrate a high degree of similarity between the mode shapes of the RRP active and passive parts, thereby indicating that the RRP phenomenon does not interfere with the MAC calculation results. Consequently, multiple damages are identified as the primary cause of modal aliasing in high-frequency modes for pipes.

The results of the modal hammer excitation tests demonstrate that the occurrence of RRPs could facilitate the identification of Level 1 damage for multiple-damage pipes. The difference between the active part and the passive part of the i-th pair of RRP is represented by ΔF_i. By analysing the difference, a qualitative relationship with the angle between the damage centroids and the number of damages is identified. As shown in Table 5, a negative correlation is observed between the absolute value of the 180° difference for multiple damages and the range, *i.e.*, a larger range corresponds to a smaller angle between the two damage centroids. The number of damages, on the contrary, could be roughly estimated by the magnitude of the mean; a larger mean value suggests a greater number of damages.

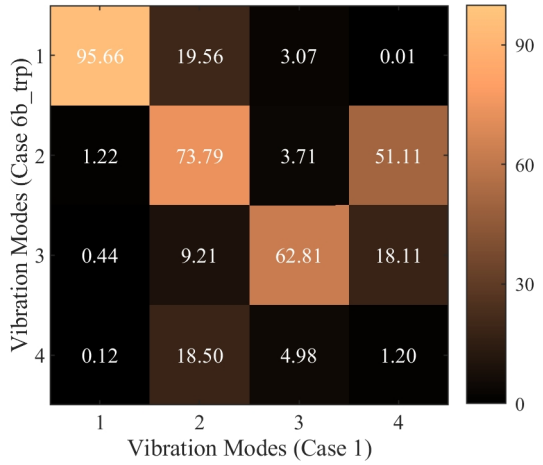

Fig. 13. MAC calculation results of vibration mode shapes for triple-damage pipes and an undamaged pipe.

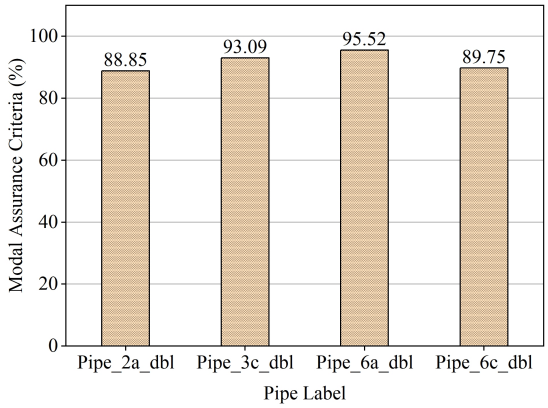

Fig. 14. MAC of vibration mode shapes for active and passive parts of RRP.

Table 5. Difference, range and average of RRP frequency of five damaged pipes.

Pipe Label	**Mode 1** ΔF_1 **(%)**	**Mode 2** ΔF_2 **(%)**	**Mode 3** ΔF_3 **(%)**	**Range** $R_{\Delta F}$ **(%)**	**Mean** $AVG_{\Delta F}$ **(%)**
2	25.9	30.3	16.4	13.9	24.2
3	27.9	28.8	18.8	10.0	25.2
4	28.2	27.5	17.0	11.2	24.2
5	26.6	31.7	16.8	14.9	25.0
6	26.8	35.6	20.9	14.7	27.8

3.3. Training of the One-vs-Rest model and damage localisation

Model training is based on the 1000 sets of simulation results detailed in Section 2.3. The damage localisation band, where the damage is situated, is represented in matrix form. Damage localisation bands the exhibit damage are marked as 1, while others are marked as 0, resulting

in an annotation on the damage localisation band such as [0, 1, 0, 0, 0, 1]. This labelled damage localisation band served as the model's output. Given that only the ratio of the RRP active and passive components, along with the specific RRP values, could be acquired during the modal excitation tests, these variables are designated as the input of the model. The relationship between modal frequencies and damage localisation bands is established using a One-vs-Rest model.

Numerous One-vs-Rest models are currently available. Five algorithms demonstrating superior performance are selected for comparative analysis and the model predictions are evaluated based on the Macro-F1 score. These five algorithms are: LR, SVM, RF, XGB, and *Multilayer Perceptron* (MLP). Except for the MLP, the hyperparameters for the other four algorithms are maintained at their default settings. The optimisation function for the MLP is AdamW, with an initial learning rate set to 0.001. The hidden layer architecture of the MLP consisted of four layers, with neuron counts of 256, 128, 64, and 32, respectively; the activation function for each layer is ReLu. The final Macro-F1 scores, recall rates, and precision values for the five algorithms in the test set are presented in Fig. 15 and Table 6. The MLP achieved the highest overall Macro-F1 score (0.8131) among the five algorithms, as shown in Fig. 15(a). Consequently, the MLP model will be used for subsequent assessment of accuracy of Level 2 damage localisation.

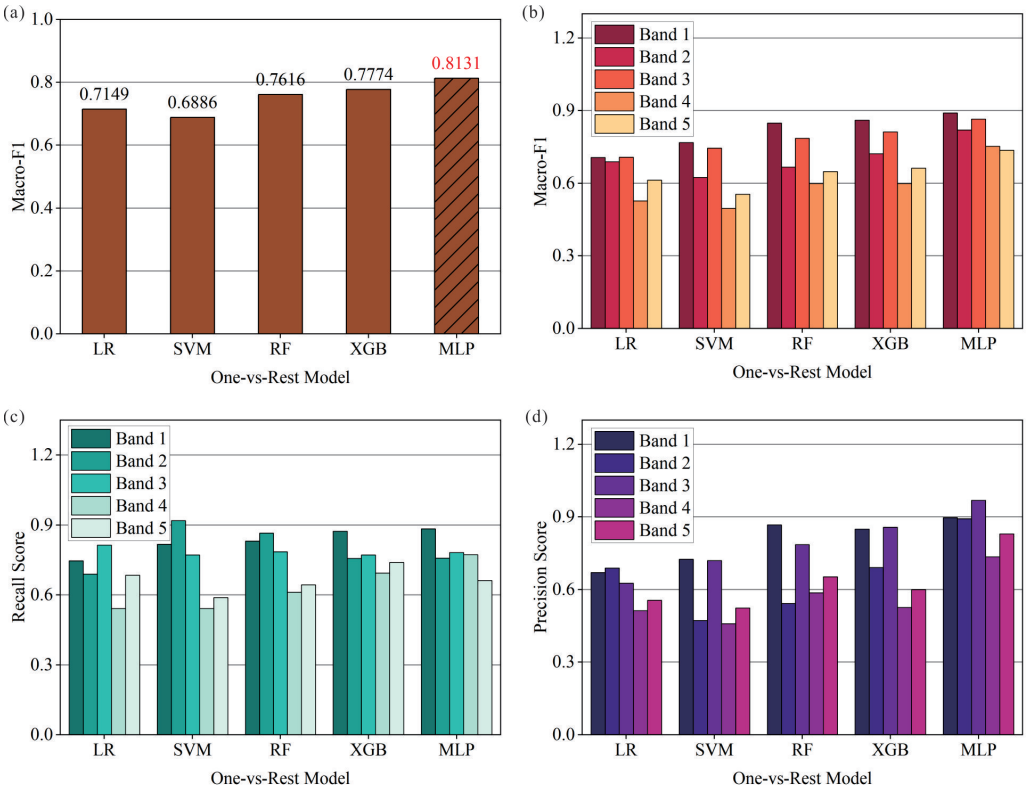

Fig. 15. Evaluation results of five algorithms on the test set: (a) overall Macro-F1 score, (b) Macro-F1 score, (c) recall score, (d) precision score.

Table 6. Evaluation of five algorithms in five damage localisation bands in the test set

Damage Localisation Band	Evaluation Indicators	LR	SVM	RF	XGB	MLP
Band 1	Macro-F1	0.7067	0.7682	0.8489	0.8611	0.8905
	Recall Score	0.7465	0.8169	0.8310	0.8732	0.8841
	Precision Score	0.6709	0.7250	0.8676	0.8493	0.8971
Band 2	Macro-F1	0.6892	0.6239	0.6667	0.7226	0.8197
	Recall Score	0.6892	0.9189	0.8649	0.7568	0.7576
	Precision Score	0.6892	0.4722	0.5424	0.6914	0.8929
Band 3	Macro-F1	0.7081	0.7448	0.7857	0.8120	0.8652
	Recall Score	0.8143	0.7714	0.7857	0.7714	0.7821
	Precision Score	0.6264	0.7200	0.7857	0.8571	0.9683
Band 4	Macro-F1	0.5270	0.4968	0.5986	0.5988	0.7531
	Recall Score	0.5417	0.5417	0.6111	0.6944	0.7722
	Precision Score	0.5132	0.4588	0.5867	0.5263	0.7349
Band 5	Macro-F1	0.6135	0.5548	0.6483	0.6626	0.7368
	Recall Score	0.6849	0.5890	0.6438	0.7397	0.6622
	Precision Score	0.5556	0.5244	0.6528	0.6000	0.8305

3.4. Point cloud voxelisation and damage quantification

After the completion of Level 2 damage localisation, scouldning of the point cloud for the corresponding damage localisation band is required. Based on the depth information from the point cloud, the centroid position is further determined to be 203.56 mm. The volume of the damaged pipe section is then predicted using this damage centroid position and the results of point cloud voxelisation. The registration, fusion, and voxelisation process of point cloud data is shown in Fig. 16. The two point cloud datasets for registration originated from two distinct cameras and are represented by different colours. The RMSE for registration is 2.96 mm, and the quality of the point cloud is discernibly improved post-fusion. By calculating the distance deviation between the actual point cloud and the ideal pipe surface, the approximate extent and volume of the damage could be effectively estimated. Damaged points are coloured red, while normal points are coloured blue. The setting of the voxel size is based on the average density of all points in the fused point cloud. The average density of the fused point cloud is 4.03 mm. To avoid issues of point cloud discretisation and to ensure volume continuity, the voxel size is set to be slightly larger than the average point cloud density, specifically 4.04 mm. Finally, after point cloud voxelisation, the volume of the damaged pipe section is calculated to be 37915.08 mm^3. This value will be used for the subsequent evaluation of accuracy of Level 3 damage quantification.

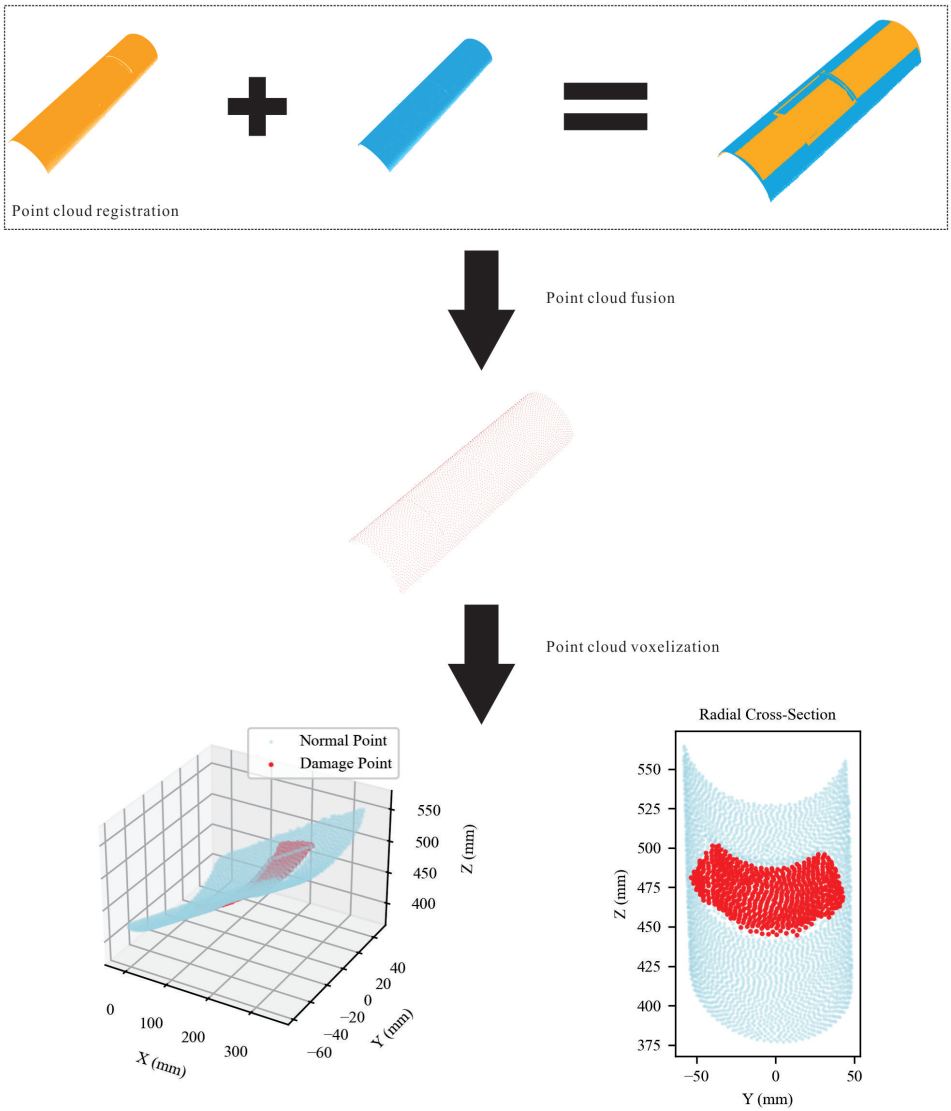

Fig. 16. Flowchart of the results of point cloud processing for a damaged pipe.

4. Accuracy of damage identification

The assessment of pipe damage identification in this paper encompasses damage detection, localisation, and quantification. Among these, damage identification is predicated on the presence or absence of the RRP phenomenon. The results of the modal test presented in Section 3.2 indicate that all five multiple-damage pipes exhibited damage. Furthermore, a qualitative determination of the distance between two damage centroids and the number of damages could be performed. As the localisation and quantification of multiple damages merely involve a repetition of the operations for a single damage, the results for M_{d1} are presented as an illustrative example for

damage localisation. Based on the MLP model trained in Section 3.3, its output is determined to be [0,1,0,0,1], signifying the presence of damage in Band 2 and Band 5. M_{d1} is indeed situated in Band 2, and the point cloud depth information indicated its specific location at 203.56 mm, which is remarkably close to the actual position of 200 mm, as shown in Table 2. Consequently, the error for localisation of Level 2 damage is only 1.78%. The damage volume predicted by point cloud voxelisation in Section 3.4 is 37915.08 mm^3. The actual damage volume, calculated after modelling in SolidWorks, is 38877.209 mm^3, indicating that the error for Level 3 damage quantification is merely 2.47%.

5. Conclusions

This study proposes a multimodal baseline-free pipe multiple damage identification method. The presence of damage is effectively determined through observation of the RRP phenomenon in multiple-damage pipes, thus achieving Level 1 damage identification. A model establishing the relationship between modal frequencies and damage regions is constructed based on a *Multilayer Perceptron* (MLP). Testing revealed a Macro-F1 score of 0.8131 on the test set, indicating that modal frequencies could effectively ascertain the approximate location of damage. Furthermore, by integrating depth information from a point cloud acquired via LSL, the precise position of the damage centroid could be accurately determined, thus achieving Level 2 damage identification. Finally, point cloud registration and fusion techniques are employed to enhance point cloud quality. By combining point cloud voxelisation methods with the known damage centroid position, the extent and volume of the damage are calculated, thereby realising Level 3 damage identification. The experimental results have demonstrated that the error in damage quantification is only 2.47%. Additionally, it is found that the absolute value of the 180°difference between multiple damages and their centroids exhibits a negative correlation with the damage range *i.e.*, a larger range corresponds to a smaller angle between the two damage centroids. The number of damages could be roughly estimated by the mean value of the damage region; a larger mean value suggests a greater number of damages. This method is particularly well-suited for early damage identification; when the RRP phenomenon is not pronounced, it may indicate that the damage is in a complex state or of a smaller scale. Compared to traditional methods, the present study significantly enhances identification accuracy and reduces identification costs. By directly focusing LSL on the damaged area and eliminating the need for a baseline, identification efficiency is markedly improved. Through this strategy of integrating multi-modal technology with ML, the proposed method not only offers higher precision than traditional damage identification methods but also provides data support for the implementation of intelligent SHM systems.

Acknowledgements

This work is supported by the National Natural Science Foundation of China [Grant no. 52575175].

References

[1] Gu, Y., Liao, Z., Gu, M., Li, Z., Jia, J., & Tu, S.-T. (2023). A novel coupling method for ultrasonic transducer based on pressureless sintering of nano-Ag. *Journal of Materials Research and Technology*, *28*, 2478–2487. https://doi.org/10.1016/j.jmrt.2023.12.167

[2] Gu, Y., Wang, M., Hou, Z., Jia, J., & Tu, S. (2024). Effect of the paste spreadability on ultrasonic transducer fabricated by pressureless sintering of nano-Ag. *Measurement*, *236*, 115110. https://doi.org/10.1016/j.measurement.2024.115110

[3] Sharma, V. B., Tewari, S., Biswas, S., Lohani, B., Dwivedi, U. D., Dwivedi, D., Sharma, A., & Jung, J. P. (2021). Recent advancements in AI-enabled smart electronics packaging for structural health monitoring. *Metals*, *11*(10), 1537. https://doi.org/10.3390/met11101537

[4] Sharma, V. B., Singh, K., Gupta, R., Joshi, A., Dubey, R., Gupta, V., Bharadwaj, S., Zafar, M. I., Bajpai, S., Khan, M. A., Srivastava, A., Pathak, D., & Biswas, S. (2021). Review of structural health monitoring techniques in pipeline and wind turbine industries. *Applied System Innovation*, *4*(3), 59. https://doi.org/10.3390/asi4030059

[5] Sharma, V. B., Tewari, S., Biswas, S., & Sharma, A. (2023). A comprehensive study of techniques utilised for structural health monitoring of oil and gas pipelines. *Structural Health Monitoring*, *23*(3), 1816–1841. https://doi.org/10.1177/14759217231183715

[6] Hassan, S. I., Dang, L. M., Mehmood, I., Im, S., Choi, C., Kang, J., Park, Y., & Moon, H. (2019). Underground sewer pipe condition assessment based on convolutional neural networks. *Automation in Construction*, *106*, 102849. https://doi.org/10.1016/j.autcon.2019.102849

[7] Su, T.-C., Yang, M.-D., Wu, T.-C., & Lin, J.-Y. (2011). Morphological segmentation based on edge detection for sewer pipe defects on CCTV images. *Expert Systems with Applications*, *38*(10), 13094–13114. https://doi.org/10.1016/j.eswa.2011.04.116

[8] Bayissa, W. L., Haritos, N., & Thelandersson, S. (2007). Vibration-based structural damage identification using wavelet transform. *Mechanical Systems and Signal Processing*, *22*(5), 1194–1215. https://doi.org/10.1016/j.ymssp.2007.11.001

[9] Liu, B., Lu, H., Wu, Z., Li, S., & Liu, Q. (2020). Detection scheme of volume of repair of engineering equipment based on line structured light. *Volume 2: Manufacturing Processes; Manufacturing Systems; Nano/Micro/Meso Manufacturing; Quality and Reliability*. https://doi.org/10.1115/msec2020-8237

[10] Wenbin, M., Zhiwen, D., Xiang, L., & Hang, Z. (2024) Study on submarine pipeline suspension internal detection based on vibration response analysis, *Chinese Journal of Engineering Design 31(03)*, 348-356. https://doi.org/10.3785/j.issn.1006-754X.2024.03.170

[11] Wang, M., Gu, Y., Fu, Y., Zhu, Y., Jia, J., & Tu, S. (2024). Baseline-free damage identification in clamped-clamped pipes based on regional resonance pairs. *International Journal of Pressure Vessels and Piping*, 105416. https://doi.org/10.1016/j.ijpvp.2024.105416

[12] Singh, A., & Kaloni, S. (2023). Unsupervised ambient vibration-based feature extraction for structural damage detection. In *Communications in Computer and Information Science,* 554–565. https://doi.org/10.1007/978-3-031-37940-6_45

[13] Timilsena, H., Singh, A., Kumar, M., & Goyal, S. (2024). Comparative study of seismic analysis of RCC building using IS Code 1893:2016 (Part-1) and Nepal Building Code 105:2020. In *2024 1st International Conference on Sustainable Computing and Integrated Communication in Changing Landscape of AI (ICSCAI)*, 1–14. https://doi.org/10.1109/icscai61790.2024.10866768

[14] Xingsheng, X., Guoliang, H., Wencai, Z., Lifan, Y.,& Gang, L. (2024) Research on power generation performance of vibration energy collecting magnetorheological damper, *Chinese Journal of Engineering Design 31(02),* 201–209. https://doi.org/10.3785/j.issn.1006-754X.2024.03.139

[15] Fang, X., Li, Q., Zhu, J., Chen, Z., Zhang, D., Wu, K., Ding, K., & Li, Q. (2022). Sewer defect instance segmentation, localisation, and 3D reconstruction for sewer floating capsule robots. *Automation in Construction*, *142*, 104494. https://doi.org/10.1016/j.autcon.2022.104494

[16] Ma, D., Liu, J., Fang, H., Wang, N., Zhang, C., Li, Z., & Dong, J. (2021). A multi-defect detection system for sewer pipelines based on StyleGAN-SDM and fusion CNN. *Construction and Building Materials*, *312*, 125385. https://doi.org/10.1016/j.conbuildmat.2021.125385

[17] Zhou, Y., Ji, A., & Zhang, L. (2022). Sewer defect detection from 3D point clouds using a transformer-based deep learning model. *Automation in Construction*, *136*, 104163. https://doi.org/10.1016/j.autcon.2022.104163

[18] Vandiver, J. K. (1975). Detection of structural failure on fixed platforms by measurement of dynamic response. *Offshore Technology Conference*. https://doi.org/10.4043/2267-ms

[19] Yuen, M. (1985). A numerical study of the eigenparameters of a damaged cantilever. *Journal of Sound and Vibration*, *103*(3), 301–310. https://doi.org/10.1016/0022-460x(85)90423-7

[20] Vaish, R., Dwivedi, U., Tewari, S., & Tripathi, S. (2021). Machine learning applications in power system fault diagnosis: Research advancements and perspectives. *Engineering Applications of Artificial Intelligence*, *106*, 104504. https://doi.org/10.1016/j.engappai.2021.104504

[21] Tewari, S., & Dwivedi, U. (2018). Ensemble-based big data analytics of lithofacies for automatic development of petroleum reservoirs. *Computers & Industrial Engineering*, *128*, 937–947. https://doi.org/10.1016/j.cie.2018.08.018

[22] Nguyen, H. D., Dao, N. D., & Shin, M. (2025). Capability of machine learning to predict seismic damage states of reinforced concrete wall structures. *Journal of Building Engineering*, 112620. https://doi.org/10.1016/j.jobe.2025.112620

[23] Li, L., Chang-Richards, A., Boston, M., Elwood, K., & Brunsdon, D. (2025). A machine learning-supported rapid classification of building damage following the 2010-2011 Canterbury earthquakes. *Journal of Building Engineering*, 112807. https://doi.org/10.1016/j.jobe.2025.112807

[24] Wu, X., Ghaboussi, J., & Garrett, J. (1992). Use of neural networks in detection of structural damage. *Computers & Structures*, *42*(4), 649–659. https://doi.org/10.1016/0045-7949(92)90132-j

[25] Worden, K., & Lane, A. J. (2001). Damage identification using support vector machines. *Smart Materials and Structures*, *10*(3), 540–547. https://doi.org/10.1088/0964-1726/10/3/317

[26] Agrawal, A. K., & Chakraborty, G. (2018). Structural damage detection by integrating short time Fourier transform, principal component analysis and logistic regression. In *CRC Press eBooks* (pp. 971–976). https://doi.org/10.1201/9781351174664-122

[27] Zhou, Q., Ning, Y., Zhou, Q., Luo, L., & Lei, J. (2012). Structural damage detection method based on random forests and data fusion. *Structural Health Monitoring*, *12*(1), 48–58. https://doi.org/10.1177/1475921712464572

[28] Leon-Medina, J. X., Anaya, M., Parés, N., Tibaduiza, D. A., & Pozo, F. (2021). Structural damage classification in a jacket-type wind-turbine foundation using principal component analysis and extreme gradient boosting. *Sensors*, *21*(8), 2748. https://doi.org/10.3390/s21082748

[29] Sharma, V. B., & Biswas, S. (2020). Modern Smart Sensing Technology in Structural Health Monitoring. In *2020 International Conference on Smart Innovations in Design, Environment, Management, Planning and Computing (ICSIDEMPC)* (pp. 105–108). https://doi.org/10.1109/icsidempc49020.2020.9299595

[30] Huang, M., Xu, Z., Cai, C., Chen, D., Yin, W., & He, X. (2025). Vibration-based damage detection in laminated composite plates: a novel approach using superposition of higher-order derivatives of mode shapes. *Structural Health Monitoring*. https://doi.org/10.1177/14759217251334803

[31] Alvandi, A., & Cremona, C. (2005). Assessment of vibration-based damage identification techniques. *Journal of Sound and Vibration*, *292*(1–2), 179–202. https://doi.org/10.1016/j.jsv.2005.07.036

[32] Sharma, V. B., Dubey, R., Bhatt, A., Bharadwaj, S., Srivastava, A., & Biswas, S. (2022). A Method For Extracting Deformation Features from Terrestrial Laser Scanner 3d Point Clouds Data in Rgipt Building. *The International Archives of the Photogrammetry, Remote Sensing and Spatial Information Sciences*, *XLIII-B2-2022*, 267–272. https://doi.org/10.5194/isprs-archives-xliii-b2-2022-267-2022

[33] Wang, W., Niu, H., Qiu, S., Wang, J., Luo, Y., Zaheer, Q., & Peng, J. (2024). Railway-fastener point cloud segmentation and damage quantification based on deep learning and synthetic data augmentation. *Journal of Computing in Civil Engineering*, *39*(2). https://doi.org/10.1061/jccee5.cpeng-6026

[34] Liu, X., Yu, B., Cai, D., & Wang, R. (2024). Potential damage area detection of bridges based on single-temporal point cloud. *Measurement Science and Technology*, *36*(1), 015214. https://doi.org/10.1088/1361-6501/ad9041

[35] Li, N., Wu, R., Li, H., Wang, H., Gui, Z., & Song, D. (2023). M2FNET: Multimodal fusion network for airport runway subsurface defect detection using GPR data. *IEEE Transactions on Geoscience and Remote Sensing*, *61*, 1–16. https://doi.org/10.1109/tgrs.2023.3308205

[36] Hinks, T., Carr, H., Truong-Hong, L., & Laefer, D. F. (2012). Point Cloud Data Conversion into Solid Models via Point-Based Voxelisation. *Journal of Surveying Engineering*, *139*(2), 72–83. https://doi.org/10.1061/(asce)su.1943-5428.0000097

[37] Yoon, Y., Lee, J., Yoo, S., & Choi, H. (2002). A New Method for In-plane Vibration Analysis of Circular Rings with Widely Distributed Deviation. *Journal of Sound and Vibration*, *254*(4), 787–800. https://doi.org/10.1006/jsvi.2001.4124

[38] Allaei, D., Soedel, W., & Yang, T. (1986). Natural frequencies and modes of rings that deviate from perfect axisymmetry. *Journal of Sound and Vibration*, *111*(1), 9–27. https://doi.org/10.1016/s0022-460x(86)81419-5

[39] Fox, C. (1990). A simple theory for the analysis and correction of frequency splitting in slightly imperfect rings. *Journal of Sound and Vibration*, *142*(2), 227–243. https://doi.org/10.1016/0022-460x(90)90554-d

[40] Ewins, D. J. (2009). Modal testing: Theory, Practice and Application. John Wiley & Sons.

Mingyuan Wang received his M.Eng. degree in materials science and engineering from Qilu University of Technology (Shandong Academy of Sciences) in Shandong, China, in 2023. He is currently pursuing his Ph.D. in power engineering and engineering thermophysics at East China University of Science and Technology in Shanghai, China. His research focuses on identification of pipe damage.

Yiqing Gu received his M.Eng. degree from the School of Mechanical and Power Engineering of Nanjing Tech University, Nanjing, in 2022. He is currently pursuing his Ph.D. degree at East China University of Science and Technology, Shanghai. His current research focuses on structural health monitoring.

Yaokai Li received his B.Sc. degree in process equipment and control engineering from East China University of Science and Technology in Shanghai, China in 2023. He is currently pursuing a Ph.D. in power engineering and engineering thermophysics at East China University of Science and Technology in Shanghai, China. His research focuses on ultrasonic monitoring of structural health.

Jiuhong Jia received her Ph.D. degree in mechanical design and theory from Shanghai Jiao Tong University, Shanghai, China, in 2008. Then she joined the School of Mechanical and Power Engineering of the East China University of Science and Technology as a lecturer, and then successively as an associate professor and masters' supervisor. From 2013 to 2014, Dr. Jia studied at the Department of Aeronautics of Stanford University as a visiting scholar. Her research focuses on high temperature structural safety monitoring technology.

Shan-Tung Tu received his Ph.D. degree in chemical machinery from Nanjing College of Chemical Technology in 1988, Nanjing, China. He worked as a guest scientist at the Royal Institute of Technology (KTH) from 1990 to 1993, Sweden. He was also invited to serve as a visiting professor in South Korea's Central University in 1998. He has been a Distinguished Professor of the Yangtze River Scholars Programme of East China University of Science and Technology since 2001. He was appointed as an academician of the Chinese Academy of Engineering in 2019. Professor Tu is the chairman of the Asia Pacific Committee of the International Council of Pressure Vessel Technology (ICPVT) and a member of the reliability Committee of the International Federation for the Promotion of Mechanism and Machine Science (IFToMM). His research focuses on high temperature structural integrity.